Semi-Differentiation of Reversible, Soluble-Insoluble Potential Sweep Voltammograms

View the article online for updates and enhancements.

Semi-Differentiation of Reversible, Soluble-Insoluble Potential Sweep Voltammograms

Tyler Williams,[z,*] **Ranon Fuller,**[*] **Cameron Vann, and Devin Rappleye**[**]

Department of Chemical Engineering, Brigham Young University, United States of America

Semi-differentiation, or convolution as it is sometimes known, is a mathematical technique commonly used to disentangle overlapping peaks in cyclic or linear sweep voltammograms. However, this technique is often misapplied due to misunderstandings of fractional calculus. Additionally, rigorous treatment and validation of the theory of semi-differential analysis of reversible, soluble-insoluble electrochemical reactions is lacking. Peculiarities of semi-differentiation are explored; theoretical relations for semi-differentiated voltammograms are given; the exponential nature of the theoretical curve is explored; theoretical relations are compared to experimental voltammograms for $AgNO_3$ in 1 M nitric acid at 298 K, $NiCl_2$ in LiCl at 974 K, and $LaCl_3$ in LiCl at 971 K; and the diffusion coefficients calculated from theoretical relations developed in this paper are shown to agree with those calculated using the Berzins-Delahay equation.

Semi-differentiation, a fractional calculus operation, is a powerful tool in analyzing overlapping peaks from potential sweep methods, such as linear sweep voltammetry (LSV) or cyclic voltammetry (CV), and can increase the resolution of electroanalytical measurements by narrowing and separating peaks.[1] Furthermore, semi-differentiating LSV or CV responses (typically with respect to time) yields semi-derivatives with peaks that return to a near zero baseline (i.e., no tail), which reduces the guesswork in determining the baseline for subsequent peaks. Overlapping CV peaks are commonly found in systems such as environmental samples, nuclear fuel electrorefiners, and molten salt nuclear reactors.[1–7] In these applications, electroanalytical measurements have demonstrated potential in identifying and quantifying the species in an unknown mixture.[8] However, identifying species in highly complex mixtures remains a key challenge because these mixtures may contain many unknown analytes whose signals overlap. Semi-differentiation can be a valuable tool in resolving signals in highly complex, multi-component mixtures. In molten salts, semi-differentiation has been applied to separate and analyze overlapping reduction peaks for U^{3+} and Pu^{3+};[9] La^{3+} and Gd^{3+};[5] U^{3+} and Mg^{2+};[10] Nd^{2+} and Nd^{3+};[11] U^{3+}, Mg^{2+} and Gd^{3+};[3] Ti and Nb ions;[12] W oxides;[13] and lanthanum ions,[14] though this list is not exhaustive.

The semi-derivatives of electrochemically reversible and electrochemically irreversible (hereafter referred to as reversible and irreversible, respectively) soluble-soluble electrochemical reactions in potential sweep voltammograms has been established for decades.[15–17] In contrast to the maturity of semi-differential analysis for soluble-soluble reactions, a well-established theory for soluble-insoluble electrochemical reactions has yet to be realized. Tylka et al. have posited a potential solution for reversible, soluble-insoluble peaks in potential sweep voltammograms, but it consisted of a cursory derivation and was not rigorously validated against experimental data.[9] Despite this initial contribution, demonstrated improvements in signal resolution, and the growing use of semi-differential CV analysis, the semi-derivative of soluble-insoluble reactions is still not well understood. This paper rigorously derives and validates the theoretical framework for semi-differentiated peaks in CV and LSV for reversible, soluble-insoluble reactions and seeks to improve the electrochemist's understanding of the semi-derivative mathematical operator to enable broader and more consistent adaptation of semi-differential analysis to soluble-insoluble reactions.

Theory

The semi-derivative operator ($\mathcal{D}_a^{1/2}$) can be misapplied because fractional calculus operators are unfamiliar. In our experience, newcomers often overestimate similarities between $\mathcal{D}$,[1] commonly notated as $\partial/\partial x$), while also underestimating similarities between $\mathcal{D}_a^m$), which operates on a function, $f(x)$, in the following manner:

$$\mathcal{D}_a^m f(x) = \frac{1}{\Gamma(1-m)}\left(f(a)(x-a)^{-m} + \int_a^x f'(t)(x-t)^{-m}dt \right) \quad [1]$$

where m is the order of the differentiation and must be a positive real number; a is the initial point from which you consider the function $f(x)$; Γ is the gamma function, which can be thought of as a continuous factorial function; and x is the point at which you are evaluating $\mathcal{D}_a^m f(x)$. Notice that the semi-derivative at x is dependent on the slope and magnitude of $f(x)$ not only at x, but everywhere from a to x. On this domain, a fractional derivative has a sense of memory.

To demonstrate several properties of the semi-derivative, the operators $\mathcal{D}^0$ (which returns the original function it acts upon), $\mathcal{D}_0^{1/2}$, $\mathcal{D}_\pi^{1/2}$, and $\mathcal{D}^1$ are applied to the functions $f(x) = sin(x)$ and $g(x) = sin(x) + 10$. The solutions of these operations are given in Table I and shown graphically in Fig. 1. Although zero is not a valid m for Eq. 1, the identity operation is trivial.

In Fig. 1, one can observe how the operator $\mathcal{D}_a^{1/2}$ is a hybrid of $\mathcal{D}^0$ and $\mathcal{D}^1$. In Fig. 1 (top), this behavior is manifested as a $-\pi/4$ phase shift instead of the 0 and $-\pi/2$ shifts for $\mathcal{D}^0 f(x)$ and $\mathcal{D}^1 f(x)$, respectively. In Fig. 1 (bottom), this hybrid behavior is manifested in the dependence of $\mathcal{D}_a^{1/2} g(x)$ on $\mathcal{D}^0 g(x)$ and $\mathcal{D}^1 g(x)$.

Both Figs. 1 (top) and 1 (bottom) demonstrate the impact of the choice of a. In Fig. 1 (top), this behavior is manifested by a difference in magnitude between $\mathcal{D}_0^{1/2} f(x)$ and $\mathcal{D}_\pi^{1/2} f(x)$. Figure 1 (bottom) also shows a greater difference in magnitude initially and clearly demonstrates a difference in phase shift between $\mathcal{D}_0^{1/2} g(x)$ and $\mathcal{D}_\pi^{1/2} g(x)$. These effects diminish as x diverges from a. Hence, in semi-differentiation, the initial point (a) matters, in addition to the magnitude and functional form of the original function.
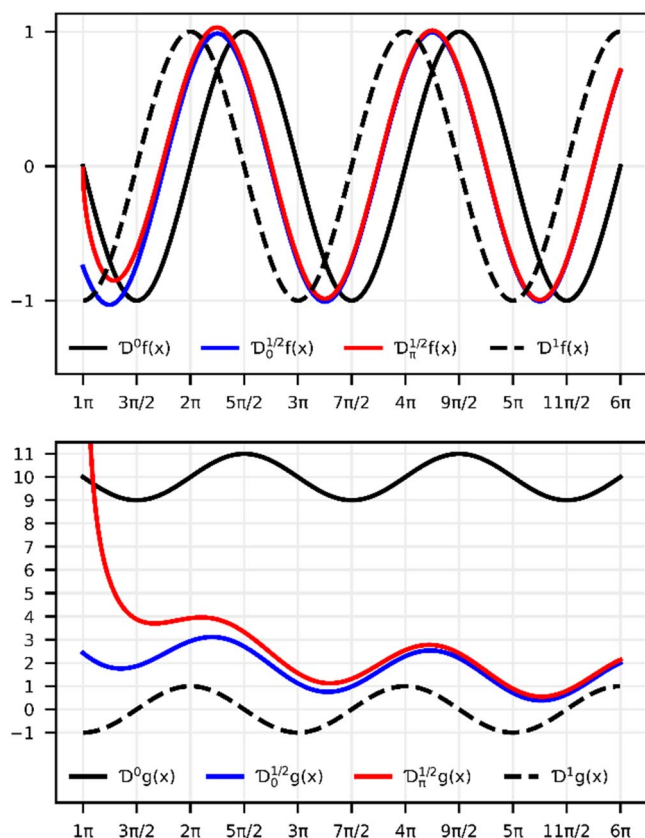
*Electrochemical Society Student Member.
**Electrochemical Society Member.
zE-mail: wtylerb@byu.edu

Table I. Solutions to various operations on $f(x) = sin(x)$ and $g(x) = sin(x) + 10$.

$\mathcal{D}^0 f(x)$	$sin(x)$
$\mathcal{D}_0^{1/2} f(x)$	$\pi^{-1/2} \int_0^x cos(t)(x-t)^{-1/2} dt$
$\mathcal{D}_\pi^{1/2} f(x)$	$\pi^{-1/2} \int_\pi^x cos(t)(x-t)^{-1/2} dt$
$\mathcal{D}^1 f(x)$	$cos(x)$
$\mathcal{D}^0 g(x)$	$sin(x) + 10$
$\mathcal{D}_0^{1/2} g(x)$	$\pi^{-1/2} \left(10x^{-1/2} + \int_0^x cos(t)(x-t)^{-1/2} dt \right)$
$\mathcal{D}_\pi^{1/2} g(x)$	$\pi^{-1/2} \left(10(x-\pi)^{-1/2} + \int_\pi^x cos(t)(x-t)^{-1/2} dt \right)$
$\mathcal{D}^1 g(x)$	$cos(x)$

Figure 1. A series of operators applied to $f(x) = sin(x)$ (top) and $g(x) = sin(x) + 10$ (bottom).

The properties of $\mathcal{D}_a^{1/2}$, demonstrated in this section, indicate that for the best agreement between theory and experiment, current (i) vs potential (E) curves should match theoretical assumptions as closely as possible. For the Berzins-Delahay model, which is typically used to evaluate soluble-insoluble electrochemical reactions, these assumptions are: (1) no initial current ($i(t=0)=0$), (2) the peak begins at the equilibrium potential ($E(t=0) = E_{eq}$), (3) semi-infinite linear diffusion, and (4) activity of reduced species (i.e., deposit) is constant and equal to one.[19] Therefore, i vs E curves should be corrected to remove background (e.g., non-faradaic) current and cropped to only show data after E_{eq}.

Semi-differentiated reversible linear sweep voltammograms.— A notation system is helpful when discussing semi-differentiated CV or LSV curves for soluble-insoluble pairs. While the semi-derivative for the soluble-soluble pair has a distinguishing feature (i.e., a peak), it does not for the soluble-insoluble pair. Therefore, in this work, subscripts reference the original curve, even when used with the semi-integrated current (m) or the semi-differentiated current (e). In terms of potential, these subscripts reference the equilibrium potential (E_{eq}); the peak potential (E_p), where i experiences a peak (i_p) during CV or LSV; the half-peak potential ($E_{p/2}$), where $i_p/2$ is experienced on the front half of a peak; and the reversible half-wave potential ($E_{1/2}$), the potential where half of the diffusion limited current (i_d) is experienced during sampled-current voltammetry. Table II lists useful theoretical relations that can be used to find or calculate distinguishing features of CV or LSV plots. Note that the soluble-insoluble relations are only valid for a system that satisfies the same assumptions of the Berzins-Delahay equation.

The symbols in Table II are assigned the following meaning: $E^{0'}$ is the formal potential, R is the ideal gas constant, T is the absolute temperature, n is the number of exchanged electrons, F is Faraday's constant, D is the diffusion coefficient, C^O is the standard reference concentration of 1 M, C^* is the bulk concentration, C is the concentration at the electrode surface, and subscripts O and R indicate the oxidized and reduced species, respectively.

Soluble-soluble theory.— A review of the derivation of semi-differentiated current for the soluble-soluble system can provide key context and rationale to understanding the derivation of the soluble-insoluble system. Goto and Ishii[15] derived an expression for the reversible soluble-soluble semi-derivative peak by rearranging the following relation developed by Goto and Oldham:[23]

$$E(t) = E_{1/2} + \frac{RT}{nF} ln \left(\frac{m_d}{m(t)} - 1 \right) \qquad [2]$$

where m_d is the diffusion limited semi-integral current ($m_d = nFAC_O^* D_O^{1/2}$) and A is the area of the working electrode (WE). Equation 2 was derived by assuming semi-infinite linear diffusion and electrochemical reversibility. By solving Eq. 2 for m, Goto and Ishii[15] obtained the following equation for the semi-integral current:

$$m(t) = -\frac{nFA}{2} D_O C_o^* \left[1 - tanh\left(\frac{nF}{2RT}(E(t) - E_{1/2}) \right) \right] \qquad [3]$$

Note that signs in this work maintain the IUPAC convention of reduction currents being negative. For LSV scanning negatively, a potential ramp function starting at equilibrium, E(t) is given by:

$$E(t) = E_{eq} - \nu t \qquad [4]$$

where ν is the scan rate and t is time, which is substituted into Eq. 3. After taking the derivative, Dalrymple-Alford et al.[16] derived the expression:

$$e(t) = -\frac{n^2 F^2 A C_o^* \nu}{4RT} D_O^{1/2} sech^2\left(\frac{nF}{2RT}(E(t) - E_{1/2}) \right) \qquad [5]$$

The peak, or minimum, of Eq. 5 occurs when $E = E_{1/2}$.[16] Therefore, the semi-differentiated peak potential is $E_{1/2}$, and the semi-differentiated peak height ($e_{1/2}$) is

$$e_{1/2} = -\frac{n^2 F^2 A C_o^* \nu D_O^{1/2}}{4RT}. \qquad [6]$$

In the literature, $e_{1/2}$ is often notated as e_p. However, in this work, subscripts reference the original curve, not the semi-differentiated curve. Dalrymple-Alford et al.[16] found that the peak full-width at half maximum ($w_{p/2}$) is 3.53 RT/nF.

Table II. Useful potential relations.

Soluble-Soluble[20]	Soluble-Insoluble[9,19,21,22]
$E_{eq} = E^{0'} + \dfrac{RT}{nF}ln\left(\dfrac{C_O}{C_R}\right)$	$E_{eq} = E^{0'} + \dfrac{RT}{nF}ln\left(\dfrac{C_O}{C^0}\right)$
$\|E_p - E_{p/2}\| = \dfrac{2.2RT}{nF}$	$\|E_p - E_{p/2}\| = \dfrac{0.774RT}{nF}$
$\|E_p - E_{1/2}\| = \dfrac{1.109RT}{nF}$	$\|E_p - E_{eq}\| = \dfrac{0.8540RT}{nF}$
$E_{1/2} = E^{0'} + \dfrac{RT}{nF}ln\left(\left[\dfrac{D_R}{D_O}\right]^{1/2}\right)$	$E_{1/2} = E^{0'} + \dfrac{RT}{nF}ln\left(\dfrac{C_O^*}{2C^0}\right)$ a)

a) This relation was given by Tylka et al. without citation or derivation.[9] A derivation is supplied here in the appendix.

Soluble-insoluble theory.—For soluble-insoluble pairs, the treatment above is no longer valid. Under these circumstances, the reduced species is insoluble, therefore D_R does not exist and $E_{eq} = E^{0'} + RT/(nF)ln(C_O/C^0)$. This equation assumes that the activity of the reduced species is equal to one (i.e., a pure coating of the insoluble species on the WE). Tylka et al.[9] assumed that the semi-integral current can still be related to the concentration of the oxidized species by:

$$m(t) = nFAD_O^{1/2}(C_O - C_o^*). \qquad [7]$$

Since Eq. 7 is derived from the semi-integration of Fick's first law,[24] it is reasonable to assume its application as long as the reaction is not kinetically controlled and diffusion is the dominant form of mass transport. After combining Eq. 7 with the expression for E_{eq}, Tylka then found that:

$$m(t) = -nFAC_o^*D_O^{1/2}\left\{1 - \frac{1}{2}exp\left[\frac{nF}{RT}(E(t) - E_{1/2})\right]\right\} \qquad [8]$$

Tylka et al. then differentiated Eq. 8 to obtain the semi-differentiated current. In this work, a slightly different expression is derived by substituting Eq. 4 into Eq. 8 then differentiating.

$$e(t) = -\frac{n^2F^2AC_o^*D_O^{1/2}\nu}{2RT}exp\left\{\frac{nF}{RT}(E_{eq} - \nu t - E_{1/2})\right\} \qquad [9]$$

Using the expressions for E_{eq} and $E_{1/2}$ in Table II for soluble-insoluble reactions, Eq. 9 can be transformed into

$$e(t) = -\frac{n^2F^2AC_o^*D_O^{1/2}\nu}{RT}exp\left\{\frac{nF}{RT}(-\nu t)\right\} \qquad [10]$$

and the following relations for e at different points of the curve can be determined:

$$e_{1/2} = -\frac{n^2F^2AC_O^*\nu D_O^{1/2}}{2RT} \qquad [11]$$

$$e_p = -0.4257\frac{n^2F^2AC_O^*\nu D_O^{1/2}}{RT} \qquad [12]$$

Equations 11 and 12 are proportional to A, C_O^*, and $D_O^{1/2}$. This allows researchers to develop functions for quick calculations of A (e.g., electrode depth), D_O, and C_O from the semi-differentiated current.[8]

Equations 8–12 were derived using identical assumptions to the Berzins-Delahay equation. Therefore, they are less accurate when depositing on a foreign substrate and t is low because a complete
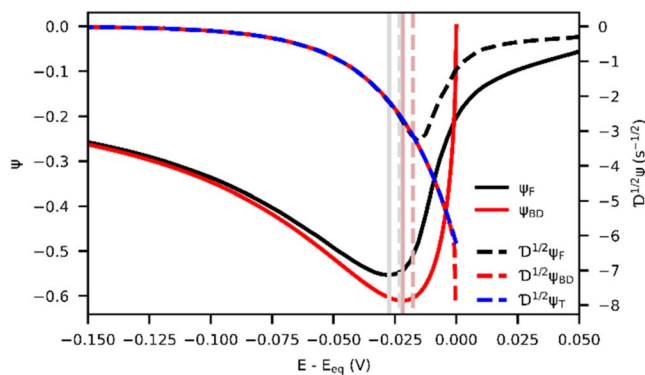

Figure 2. Calculated dimensionless currents and their semi-derivatives. $E_{1/2}$ and E_p are depicted by vertical lines with a lighter tone than their associated curves. Dotted lines depict $E_{1/2}$ and solid lines depict E_p.

monolayer of the deposit may not have formed yet. When depositing onto a foreign substance, Eq. 12 is recommended over Eq. 11 as the most reliable model because historical effects of the semi-derivative decrease and the deposit coverage on the WE increases as the initial point becomes more distant (i.e., the peak occurs later than the half-wave).

The theoretical and mathematical consistency of Eq. 10 is verified by applying the Riemann-Liouville fractional integral operator:[18]

$$J_a^m f(x) = \frac{1}{\Gamma(m)}\int_a^x f(t)(x - t)^{m-1}dt \qquad [13]$$

where m is the order of integral and must be given in a positive value. When Eq. 13 is applied to Eq. 10. with $a = 0$ and $m = 1/2$, the solution is the Berzins-Delahay equation:[19]

$$i(t) = -2AC_o^*\left[\frac{(nF)^3D_O\nu}{\pi RT}\right]^{1/2}daws\left(\left[\frac{nF\nu t}{RT}\right]^{1/2}\right), \qquad [14]$$

$$daws(\alpha) = \exp(-\alpha^2)\int_0^\alpha \exp(y^2)dy. \qquad [15]$$

An explanation of the exponential form of the solution.—Semi-differentiated currents from potential sweep voltammograms for electrodeposition (i.e., soluble-insoluble reactions) in the literature have manifested peaks, not exponential decays, when employing a foreign substrate as a WE.[3,5,9–14] At least some of the peak behavior occurs because when depositing onto a foreign substrate, the activity of the deposited layer is not equal to one initially.[20] Consider Fig. 2, where the dimensionless current (Ψ) of two theoretical models and their semi-derivatives ($\mathcal{D}^{1/2}\Psi$) are compared using the same system parameters ($\nu = 1$ V s^{-1}, $n^{-1} = 1$, $T = 298$ K, $D_O = 5 \times 10^{-5}$ cm^2 s^{-1}, $C_O^* = 3.53$ mM). The dimensionless current (Ψ) was calculated using the definition from Fatouros et al.

$$\Psi = \frac{i}{nFAC_O^*}\left[\frac{RT}{nF\nu D_O}\right]^{1/2}. \qquad [16]$$

Ψ_F (subscripted F for Fatouros) was taken from Figure 5b of Fatouros et al.'s work[25] using WebPlotDigitizer[26] and accounts for deposits with initial non-unit activity. Ψ_{BD} (subscripted BD for Berzins-Delahay) is the dimensionless form of Eq. 14 and assumes constant unit activity of the deposit. $\mathcal{D}^{1/2}\Psi_T$ is Eq. 10 normalized by Eq. 16, where e is substituted for i ($\mathcal{D}^{1/2}Kf(x) = K\mathcal{D}^{1/2}f(x)$). $\mathcal{D}^{1/2}\Psi_T$ and $\mathcal{D}^{1/2}\Psi_{BD}$ are exponential curves that agree well, which
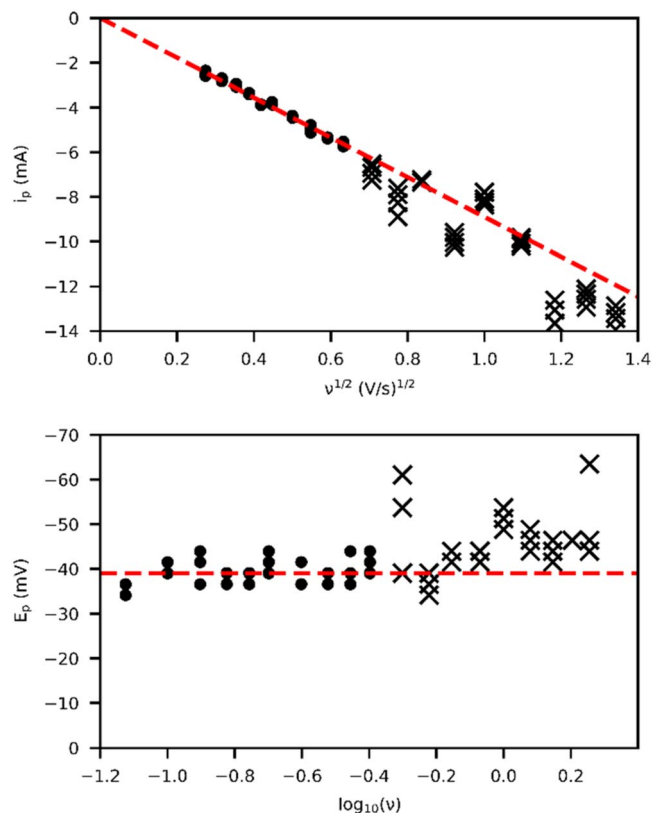
Figure 3. CV peak value correlations for i_p vs $\nu^{1/2}$ (top) and E_p vs $log_{10}(\nu)$ (bottom) of Ag(I) deposition onto Pt disk. Dots represent data analyzed in this work, the letter "x" denotes data not analyzed in this work, and dotted red lines represent a fitted line (top) and average value (bottom) of the analyzed data.

graphically shows the mathematical consistency of Eq. 10 with Eq. 14. However, $\mathcal{D}^{1/2}\Psi_F$ forms a peak.[25] Nevertheless, all the semi-derivatives agree well at both theoretical (pink vertical lines) and experimentally observed (gray vertical lines) values of $E_{1/2}$ and E_p. The comparison of $\mathcal{D}^{1/2}\Psi_F$, $\mathcal{D}^{1/2}\Psi_{BD}$, and $\mathcal{D}^{1/2}\Psi_T$ demonstrate that peaks in semi-differential analysis can result from the initial non-unit and varying activity of the deposit.

Figure 2 demonstrates that the theoretical semi-derivative ($\mathcal{D}^{1/2}\Psi_T$) relations derived and presented in this paper are not optimized for deposition onto a foreign substrate (Ψ_F) because the same assumptions as the Berzins-Delahay equation (Ψ_{BD}) are made. Therefore, potentials of Ψ_T (i.e., E_p and $E_{1/2}$) are referenced to the theoretical values of Ψ_{BD} (see Table II), not to Ψ_F. If the experimentally observed values of E_p and $E_{1/2}$ (gray lines in Fig. 2) are used as a reference with Eqs. 11 or 12, C_O^* or D_O would be underestimated. A detailed exploration of the analytical errors due to using the Berzins-Delahay equation for deposition onto foreign substrates is explored further elsewhere.[27]

Both the unit activity (*BD*) model and non-unit activity (*F*) model agree remarkably after the peak of $\mathcal{D}^{1/2}\Psi_F$ in Fig. 2. However, a reference point consistent with theory needs to be used to utilize Eqs. 11 and 12. Hence, if $E^{0'}$ and C_O are known, accurate values of D_O can be calculated using Eq. 12 if E_p is theoretically calculated from Table II, rather than using the peak of the measured *i* vs *E* curve. However, the theoretical value of E_p cannot be calculated without a known C_O. Hence, an iterative approach must be used where C_O is calculated from semi-differentiated current, then E_p is calculated, and C_O recalculated at the calculated E_p value. This is repeated until E_p and C_o no longer change between iterations. The experimentally observed E_p can serve as an initial guess to the iterative approach. Accurate calculations of D_o and C_o can be made using the semi-differentiated current, but not from the peak of the

semi-differentiated current. This peak does not have a developed and validated theoretical relationship, which is beyond the scope of this work and is planned to be addressed in a future study.

Methods

Computation.—Python 3 was used to calculate semi-derivatives by means of the *differint* Riemann-Liouville packages. These packages can calculate semi-derivatives and semi-integrals from data or user-defined functions. For the reader's benefit, example code is provided in the supplemental data.

Electrochemical experiments.—To evaluate the utility of the theoretical models formalized in this paper (Eqs. 10–12) in the case of non-unit activity deposits, D_O values were calculated using the Berzins-Delahay equation (Eqs 14–15) and Eqs. 10–12 using experimental data and compared to each other. To demonstrate the theoretical model's broad applicability, experiments were conducted in both aqueous and molten-salt environments, depositing Ag ($n = 1$), Ni ($n = 2$), and La ($n = 3$) onto foreign substrates. Ag deposition on Pt was performed in an aqueous solution. Ni and La deposition tests were performed in separate molten LiCl baths with 0.419 wt% $NiCl_2$ and 0.433 wt% $LaCl_3$, respectively, onto a 1.5 mm W rod WE. Previous works report some of the voltammograms for Ni and La for ν from 50 to 2000 mV s^{-1} and extensively detail the experimental setup.[28,29] CV measurements involving Ni and La were performed using a three-electrode set up (all made of W) and an Autolab (PGSTAT302N) potentiostat with NOVA 2.1 software, in which the CV (digital) staircase command was used with a potential step of 1 mV. To verify that the data was repeatable, three or more scans were conducted at each ν value.

Ag deposition studies were conducted in a 0.027 M $AgNO_3$ (VWR, 99%, Part No. 0377–25 G) and 1 M HNO_3 (Fisher Chemical, 68.0–70.0 wt%, Part No. A200–500) aqueous solution where Ag ions were deposited onto 5 mm diameter platinum disk (Pine Research, 99.99%, Part No. AFE3T050PT) WE, with a 0.64 mm diameter Ag wire (Alfa Aesar, 99.9%, Part No. 41390) quasi-reference electrode. The water was purified to 16 MΩ cm using a Thermo Scientific Barnstead D4631 3-Holder Water Purification System. The counter electrode was a coiled Cu wire coated with 0.02 inches of Nb wire, which in turn was coated with 0.0001 inches of Pt (Anomet Products). Electrochemical impedance spectroscopy (EIS) was used to measure the solution resistance at the open-circuit potential with 100,000 to 0.1 Hz and an amplitude of 10 mV. CV measurements were then compensated at 90% of the solution resistance value (7.24 Ω) determined by EIS. CV measurements were performed using an Autolab (PGSTAT302N) potentiostat with NOVA 2.1 software, in which the CV (digital) staircase command was used with a potential step of 2.44 mV for Ag electrodeposition. CV was applied with ν between 75 mV s^{-1} and 2000 mV s^{-1} to determine the reversible region and calculate D_O.

As previously mentioned, data should be corrected to match theoretical assumptions of no initial current and an initial potential at the equilibrium potential. The former requirement was achieved without correction due to low charging currents, the later was tested by either calculating the semi-derivative of the entire data set or only of data following E_{eq} to demonstrate the importance of this requirement. E_{eq} was determined from E_p by using the relations in Table II.

Results

Silver deposition.—The silver deposition peak currents and potentials from cyclic voltammograms for reversible values of ν are shown as dots in Fig. 3 for silver deposition on the Pt WE. As can be seen, E_p was within a ±10 mV range and not a strong function of ν for the ten lowest ν values ($\leqslant 0.5$ V s^{-1}). Figure 3 also shows that i_p was strongly linear with $\nu^{1/2}$ for these same ν values. Therefore, the system was deemed to be reversible up to at least 0.5 V s^{-1}. Hence, only data from the ten lowest ν values was used in
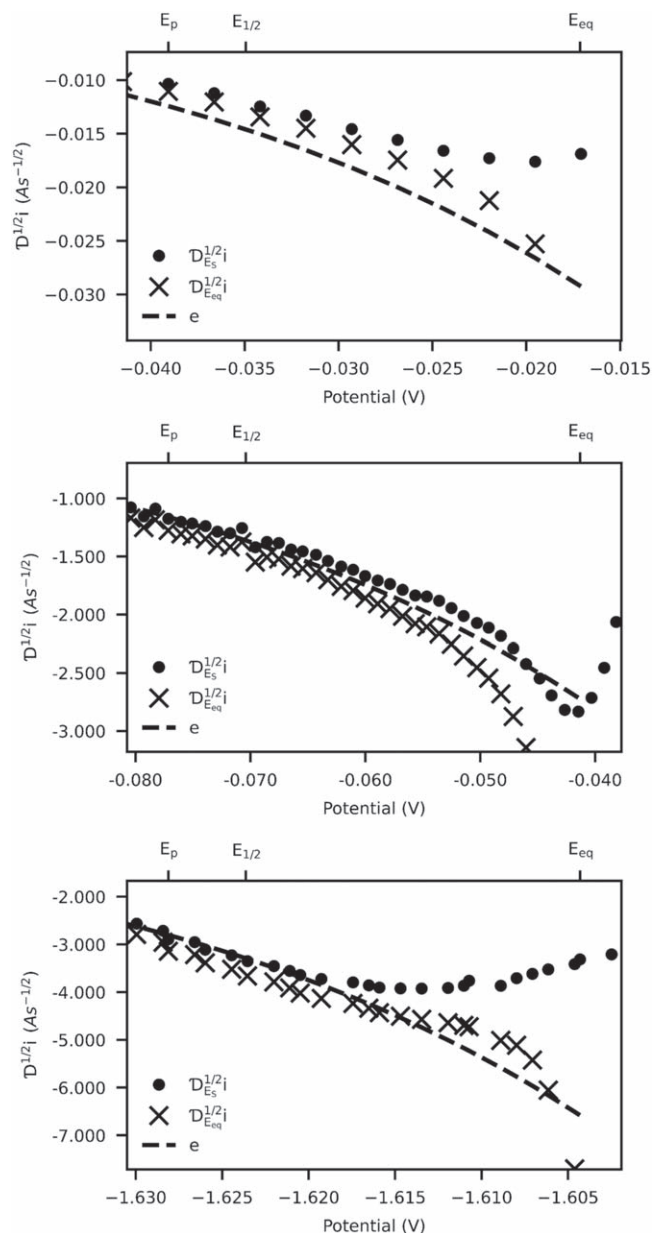
Figure 4. Comparisons of semi-differentiated i vs E curves using Eq. 10 (e), experimental data from the whole scan ($\mathcal{D}_{Es}^{1/2}i$), and data cropped to E_{eq} ($\mathcal{D}_{Eeq}^{1/2}i$). 0.027 M AgNO$_3$ in aqueous 1 M HNO$_3$, $D_O = 2.3 \times 10^{-5}$ cm^2 s^{-1}, $A = 0.2$ cm^2, $T = 298$ K, $n = 1$, $\nu = 300$ mV s^{-1}, Pt WE (top). NiCl$_2$-LiCl. $C_O^* = 4.73 \times 10^{-5}$ mol cm^{-3} (0.419 wt%), $D_O = 3.61 \times 10^{-4}$ cm^2 s^{-1}, $A = 0.66$ cm^2, $T = 974$ K, $n = 2$, $\nu = 1000$ mV s^{-1} (middle). LaCl$_3$-LiCl, $C_O^* = 2.59 \times 10^{-5}$ mol cm^{-3} (0.433 wt%), $D_O = 3.42 \times 10^{-4}$ cm^2 s^{-1}, $A = 0.66$ cm^2, $T = 971$ K, $n = 3$, $\nu = 2000$ mV s^{-1} (bottom).

Figure 5. Comparisons of e_p values from semi-differentiated i vs E curves using Eq. 10 (e_p), experimental data from the whole scan ($\mathcal{D}_{Es}^{1/2}i_p$), and data cropped to E_{eq} ($\mathcal{D}_{Eeq}^{1/2}i_p$). 0.027 M AgNO$_3$ in aqueous 1 M HNO$_3$, $D_O = 2.3 \times 10^{-5}$ cm^2 s^{-1}, $A = 0.2$ cm^2, $T = 298$ K, $n = 1$, Pt WE (top). NiCl$_2$-LiCl. $C_O^* = 4.73 \times 10^{-5}$ mol cm^{-3} (0.419 wt%), $D_O = 3.61 \times 10^{-4}$ cm^2 s^{-1}, $A = 0.66$ cm^2, $T = 974$ K, $n = 2$ (middle). LaCl$_3$-LiCl, $C_O^* = 2.59 \times 10^{-5}$ mol cm^{-3} (0.433 wt%), $D_O = 3.42 \times 10^{-4}$ cm^2 s^{-1}, $A = 0.66$ cm^2, $T = 971$ K, $n = 3$ (bottom).

the analysis hereafter. D_O was calculated to be $2.3 \pm 0.2 \times 10^{-5}$ cm^2 s^{-1} from the slope of i_p vs $\nu^{1/2}$ (dashed, red line in top plot of Fig. 3) using the following equation developed by Berzins and Delahay by evaluating Eq. 14 at its minimum.

$$i_p = -0.6105 A C_o^* \left[\frac{(nF)^3 D_O \nu}{RT} \right]^{1/2} \qquad [20]$$

Experimental validation of derived semi-differentiated current.—To evaluate the agreement between experimental data and the theoretical curve (Eq. 10), consider the semi-differentiated voltammograms shown in Fig. 4. Around $E_{1/2}$, the theoretical
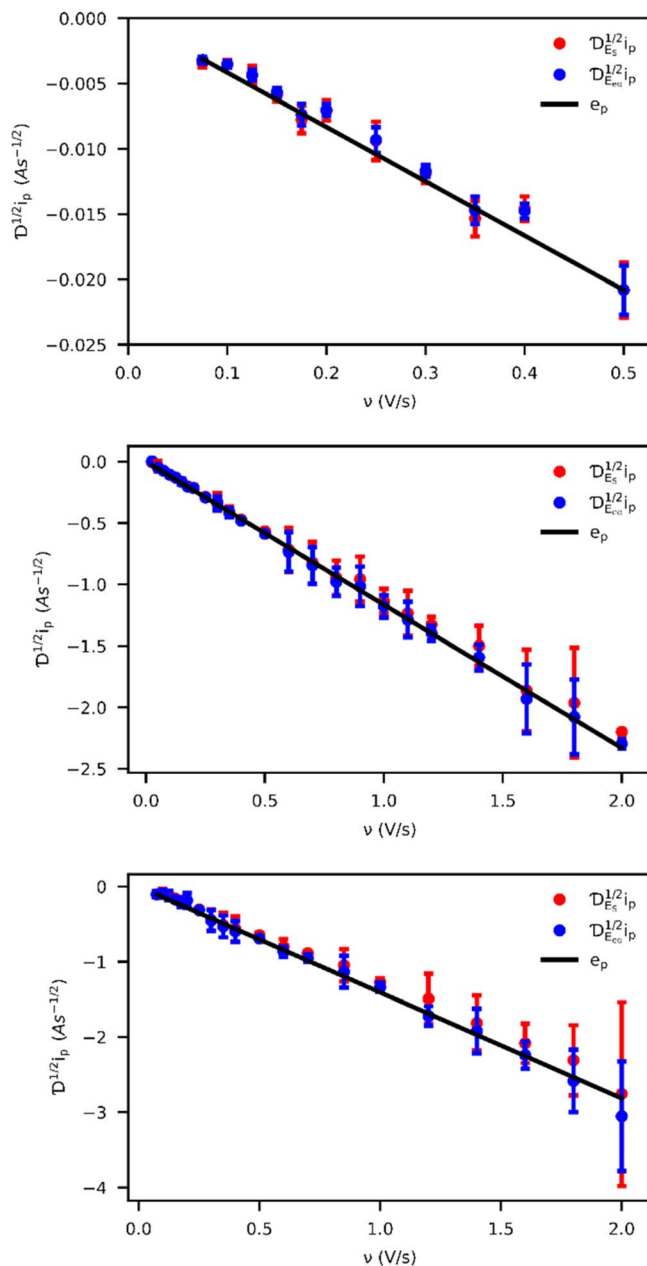
semi-differentiated current (e), and the semi-differentiated current for the entire scan ($\mathcal{D}_{Es}^{1/2}i$) and the cropped scan ($\mathcal{D}_{Eeq}^{1/2}i$) converged. This behavior was consistent regardless of ν or n. These voltammograms also demonstrate that for the soluble-insoluble pair, unlike the soluble-soluble pair, a peak does not occur at $E_{1/2}$ or any other consistent potential reference.

In Fig. 5, the linear relationship between ν and e_p is demonstrated. Mean e_p values and their 95% confidence intervals were calculated from the second, third, and fourth scans of each cyclic voltammogram. This figure also demonstrates the agreement between Eq. 12 and semi-differentiated data, despite the shifts in E_p due to depositing onto foreign substrates (see gray lines in Fig. 2).

To further verify this, D_O was calculated using Eq. 12 for each system. Using cropped scans, the mean D_O values with 95% confidence intervals are 0.20 ± 0.01, 3.43 ± 0.15, and $3.08 \pm 0.24 \times 10^{-4}$ cm^2 s^{-1}, for Ag, Ni, and La, respectively. These calculated values agree quite well with those calculated from the Berzins-Delahay equation: 0.23, 3.61, and 3.42×10^{-4} cm^2 s^{-1} for Ag, Ni and La, respectively.[28]

When comparing calculated D_O values from e_p and $e_{1/2}$, cropped data could not be used because of insufficient data resolution (i.e. for some scans, there were no data points between E_{eq} and $E_{1/2}$). Therefore, these diffusion coefficients were calculated using data from the entire scan. D_O from e_p for Ag, Ni, and La were 0.20 ± 0.01, 3.26 ± 0.12, and $2.75 \pm 0.22 \times 10^{-4}$ cm^2 s^{-1}, respectively. Values calculated from $e_{1/2}$ were 0.22 ± 0.04, 9.83 ± 1.33, and $4.51 \pm 0.39 \times 10^{-4}$ cm^2 s^{-1}, respectively. Comparing these D_O values with those calculated from the Berzins-Delahay equation demonstrates the superior consistency of using the e_p correlation (Eq. 12) instead of that belonging to $e_{1/2}$ (Eq. 11). As mentioned, this is likely due to the diminishing effects of history on the semi-derivative as the independent variable moves forward and more complete coverage of the foreign substrate by the deposit.

Discussion

Because of the impact of history on the semi-derivative, the use of semi-differentiation for decoupling overlapping peaks needs to be carefully evaluated. Future work will investigate and extend the developed semi-differentiation theory for soluble-insoluble reactions to deposition onto foreign substrates and overlapping peaks. In this paper, the usefulness of semi-derivative peaks has been called into question. If there is analytical utility in peak characteristics, it will likely contain information associated with adsorption processes in addition to concentration, thermodynamic, mass-transfer, and kinetic information.

Conclusions

A theory for the semi-derivative for a soluble-insoluble reaction in potential sweep voltammetry was formalized and demonstrated to be theoretically consistent. The derived equation does not predict a peak because the initial non-unit activity of a deposit onto a foreign substrate is ignored in the derivation. When data for deposition onto foreign substrates are properly sampled (i.e., at $E_{1/2}$ or E_p) to minimize the impact of the non-unit activity of initial deposits, the semi-derivative current agrees well with theoretically predicted values. When the theoretical assumptions (i.e., $i(t=0)=0$ and $E(t=0)=E_{eq}$) are met, the semi-derivatives take on an exponential decay form and converge with the theoretical response. The semi-derivative for soluble-insoluble peaks is given with relations that reference well-defined features of CV plots. The derived semi-derivative predicts D_O values that agree with those calculated from the Berzins-Delahay equation.

Acknowledgments

Appendix

To calculate $E_{1/2}$ for a soluble-insoluble pair, begin with Fick's second law and the following conditions:

$$\frac{\partial C_O(x, t)}{\partial t} = D_O \frac{\partial^2 C_O(x, t)}{\partial x^2} \qquad [A\cdot1]$$

$$C_O(x, 0) = C_O^* \qquad [A\cdot2]$$

$$\lim_{x \to \infty} C(x, t) = C_O^* \qquad [A\cdot3]$$

which results in the following equation when transformed into Laplace space:[20]

$$\overline{C_O}(x, s) = \frac{C_O^*}{s} + A(s) exp\left(-x\left[\frac{s}{D_O}\right]^{1/2}\right) \qquad [A\cdot4]$$

At the electrode, Eq. A·4 is

$$\overline{C_O}(0, s) = \frac{C_O^*}{s} + A(s) \qquad [A\cdot5]$$

Next, transform the Nernst equation for the soluble-insoluble pair,

$$C_O(0, t) = C^0 exp\left(\frac{nF}{RT}[E - E^{0'}]\right) \qquad [A\cdot6]$$

into the Laplace space

$$\overline{C_O}(0, s) = \frac{C^0 exp\left(\frac{nF}{RT}[E - E^{0'}]\right)}{s} \qquad [A\cdot7]$$

Equations A·5 and A·7 are then combined to find $A(s)$,

$$A(s) = \frac{C^0 exp\left(\frac{nF}{RT}[E - E^{0'}]\right) - C_O^*}{s} \qquad [A\cdot8]$$

which when plugged into Eq. A·4, creates

$$\overline{C_O}(x, s) = \frac{C_O^*}{s} + \left[\frac{C^0 exp\left(\frac{nF}{RT}[E - E^{0'}]\right) - C_O^*}{s}\right]$$
$$\times exp\left(-x\left[\frac{s}{D_O}\right]^{1/2}\right) \qquad [A\cdot9]$$

The Laplace space current (I) is related to Eq. A·9 by

$$\frac{I(s)}{nFA} = -D_O \frac{\partial \overline{C_O}(x, s)}{\partial x}\bigg|_{x=0} \qquad [A\cdot10]$$

The function is evaluated by rearranging Eq. A·10 and taking the derivative of Eq. A·9 with respect to x

$$\frac{\partial \overline{C_O}(x, s)}{\partial x}\bigg|_{x=0}$$
$$= -\frac{1}{[sD_O]^{1/2}}\left[C^0 exp\left(\frac{nF}{RT}[E - E^{0'}]\right) - C_O^*\right] \qquad [A\cdot11]$$

whose real space form is

$$\frac{\partial \overline{C_O}(x, t)}{\partial x}\bigg|_{x=0}$$
$$= -\frac{1}{[D_O \pi t]^{1/2}}\left[C^0 exp\left(\frac{nF}{RT}[E - E^{0'}]\right) - C_O^*\right] \qquad [A\cdot12]$$

The real space current is then

$$i(t) = nFA\left(\frac{D_O}{\pi t}\right)^{1/2}\left[C^0 exp\left(\frac{nF}{RT}[E - E^{0'}]\right) - C_O^*\right] \qquad [\text{A·13}]$$

whose diffusion limited form is

$$i_d = -nFAC_O^* \qquad [\text{A·14}]$$

Therefore,

$$\frac{i_D}{2} = nFA\left(\frac{D_O}{\pi t}\right)^{1/2}\left[C^0 exp\left(\frac{nF}{RT}[E_{1/2} - E^{0'}]\right) - C_O^*\right] \qquad [\text{A·15}]$$

which by combination with Eq. A·14 and rearrangement yields

$$E_{1/2} = E^{0'} + \frac{RT}{nF}ln\left(\frac{C_O^*}{2C^0}\right) \qquad [\text{A·16}]$$

ORCID

Tyler Williams https://orcid.org/0000-0002-7206-114X
Devin Rappleye https://orcid.org/0000-0002-4008-7193

References

1. M. Pałys, T. Korba, M. Bos, and W. E. van der Linden, *Talanta*, **38**, 723 (1991).
2. M. Iizuka, T. Inoue, O. Shirai, T. Iwai, and Y. Arai, *J. Nucl. Mater.*, **297**, 43 (2001).
3. H. Andrews and S. Phongikaroon, *Nucl. Technol.*, **207**, 617 (2021).
4. D. Rappleye, S.-M. Jeong, and M. Simpson, *Ann. Nucl. Energy*, **77**, 265 (2015).
5. D. Rappleye, S.-M. Jeong, and M. Simpson, *J. Electrochem. Soc.*, **163**, B507 (2016).
6. S. Paek, T.-J. Kim, G.-Y. Kim, D.-H. Ahn, S. Kim, and Y. Jung, *Int. J. Electrochem. Sci.*, **9**, 4925 (2014).
7. M. Grdeń, *J. Solid State Electrochem.*, **21**, 1045 (2017).
8. T. Williams, R. Shum, and D. Rappleye, *J. Electrochem. Soc.*, **168**, 123510 (2021).
9. M. M. Tylka, J. L. Willit, J. Prakash, and M. A. Williamson, *J. Electrochem. Soc.*, **162**, H852 (2015).
10. D. Rappleye, M. L. Newton, C. Zhang, and M. F. Simpson, *J. Nucl. Mater.*, **486**, 369 (2017).
11. K. Liu, H.-B. Tang, J.-W. Pang, Y.-L. Liu, Y.-X. Feng, Z.-F. Chai, and W.-Q. Shi, *J. Electrochem. Soc.*, **163**, D554 (2016).
12. L. P. Polyakova, P. Taxil, and E. G. Polyakov, *J. Alloys Compd.*, **359**, 244 (2003).
13. C. Zhang, D. Rappleye, A. Nelson, S. Simpson, and M. Simpson, *J. Electrochem. Soc.*, **168**, 097502 (2021).
14. M. Matsumiya, S. Matsumoto, and Z. Für, *Naturforschung A*, **59**, 711 (2004).
15. M. Goto and D. Ishii, *J. Electroanal. Chem. Interfacial Electrochem.*, **61**, 361 (1975).
16. P. Dalrymple-Alford, M. Goto, and K. B. Oldham, *J. Electroanal. Chem. Interfacial Electrochem.*, **85**, 1 (1977).
17. P. Dalrymple-Alford, M. Goto, and K. B. Oldham, *Anal. Chem.*, **49**, 1390 (1977).
18. K. Diethelm, *The Analysis of Fractional Differential Equations* (Berlin)(Springer, Berlin) (2004).
19. T. Berzins and P. Delahay, *J. Am. Chem. Soc.*, **75**, 555 (1953).
20. A. J. Bard and L. R. Faulkner, *Electrochemical Methods: Fundamentals and Applications* (New York, Wiley) 2nd ed. (2001).
21. G. Mamantov, D. L. Manning, and J. M. Dale, *J. Electroanal. Chem. 1959*, **9**, 253 (1965).
22. W. L. Miller and A. R. Gordon, *J. Phys. Chem.*, **35**, 2785 (1931).
23. M. Goto and K. B. Oldham, *Anal. Chem.*, **45**, 2043 (1973).
24. K. B. Oldham and J. Spanier, *J. Electroanal. Chem. Interfacial Electrochem.*, **26**, 331 (1970).
25. N. Fatouros, D. Krulic, and H. Groult, *J. Electroanal. Chem.*, **625**, 1 (2009).
26. A. Rohatgi, (2021), (https://automeris.io/WebPlotDigitizer).
27. D. Rappleye, *Manuscript in preparation*.
28. R. G. Fuller, T. Williams, M. Schvaneveldt, and D. Rappleye, *Eletrochim. Acta*, **414**, 140220 (2022).
29. M. Schvaneveldt, *In-Situ Chlorine Gas Generation for Chlorination and Purification of Rare Earth and Actinide Metals, Master's Thesis*, Brigham Young University (2022).